THE JOURNAL OF PHYSICAL CHEMISTRY Letters

Letter

pubs.acs.org/JPCL

Functioning Photoelectrochemical Devices Studied with Time-Resolved Terahertz Spectroscopy

Coleen T. Nemes, Christopher Koenigsmann, and Charles A. Schmuttenmaer*

Department of Chemistry and Energy Sciences Institute, Yale University, New Haven, Connecticut 06520-8107, United States

Supporting Information

ABSTRACT: Terahertz (THz) spectroscopy has been used over the years to study carrier dynamics in a large variety of semiconductor materials utilized in devices such as photoelectrochemical cells. However, due to low transmission of far-infrared radiation through conductive films, thin layers of material deposited on nonconducting substrates have been investigated rather than inside actual devices. Here, we photolithographically etch fluorine-doped tin oxide (FTO) coatings to produce a pattern analogous to a wire-grid THz polarizer, and measure a nearly 260-fold increase in percent power transmitted at 1 THz through patterned electrodes (15 μm wire width and 20 μm wire period) relative to continuous FTO films. We have employed them as visible and THz-transparent electrodes in dye-sensitized solar cells, thereby enabling us to probe the carrier dynamics of a functioning device under an applied bias and with background illumination using time-resolved THz spectroscopy. We find that the electron injection efficiency and carrier trapping time both increase as the magnitude of the negative bias voltage is increased.

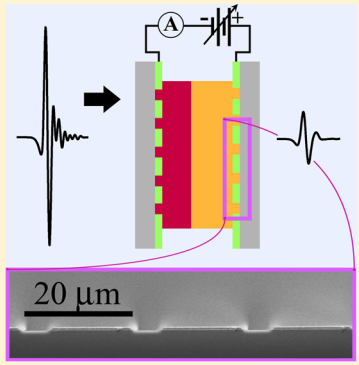

Terahertz (THz) spectroscopy has emerged over the last two decades as a versatile probe of a large variety of materials and processes. Because the transient THz electric field itself is measured rather than its power, THz spectroscopy determines frequency-dependent material properties such as the absorption coefficient, refractive index, and complex conductivity in the far-infrared region of the electromagnetic spectrum—all in a relatively straightforward manner.[1] In addition, the ultrafast nature of THz pulses is exploited when performing optical pump−THz probe studies wherein the photoinduced response of a material is characterized with subpicosecond temporal resolution. One of the most important applications of time-resolved THz spectroscopy (TRTS) has been to probe transient photoconductivity and charge carrier dynamics in a variety of materials.[1−12] More specifically, this method has been employed to characterize materials employed in a range of optoelectronic devices including organic photovoltaics,[13−18] photocatalytic water splitting cells,[12,19,20] as well as dye-sensitized[21−28] and perovskite-based solar cells.[29−31]

While THz spectroscopy has been useful for studying the materials themselves and individual components of devices, a key challenge has been the general inability to probe the active materials under operating conditions. This is largely because transparent conductive oxide (TCO) electrodes are employed, which enable transmission of visible light into or out of devices such as light emitting diodes, liquid crystal displays, and photovoltaic and photocatalytic cells. While TCOs are transparent to visible light, they are highly reflective to THz radiation and, in fact, find use as optical/THz dichroic mirrors.[32] Thus, it is not possible to probe the active material within a working device under applied bias with THz pulses. Instead, it has become common to study isolated components of these devices with THz spectroscopy, and then characterize full devices by other means. This approach has been used in studies pertaining to dye-sensitized photoelectrochemical cells,[25,27,33] photocatalytic cells,[19] as well as perovskite-based solar cells.[30] While such studies undoubtedly provide insight into charge separation and transport dynamics, there is evidence that the transient photoconductivity and charge carrier dynamics of isolated materials differ from those of materials in functioning photoelectrochemical devices within electrolyte and under an applied bias.[25,34−37]

Accordingly, we demonstrate the design, construction, and implementation of THz-transparent electrodes, and establish their utility in probing the transient photoconductivity of functioning devices under operating conditions. FTO coatings on quartz substrates are made THz-transparent by producing a wire-grid pattern using standard photolithography techniques, and we show that the transmitted power at 1 THz—determined by comparing power spectra obtained from Fourier transforms of the time-domain waveforms—is increased by a factor of ∼260 relative to a continuous FTO film. TCOs patterned in this manner transmit linearly polarized THz light with nearly 100% efficiency when the THz polarization is perpendicular to the direction of the wires, consistent with wire-grid polarizers in general. Using dye-sensitized photoelectrochemical cells as an example, we demonstrate that it is now possible to study functioning devices under an applied voltage using TRTS.

Received: July 10, 2015
Accepted: July 29, 2015
Published: July 29, 2015

DOI: 10.1021/acs.jpclett.5b01473
J. Phys. Chem. Lett. 2015, 6, 3257−3262

While we have physically constructed and characterized FTO electrodes consisting of 15 μm wide wires with a period of 20 μm (denoted 15 μm:20 μm), we also numerically simulated the THz transmission for a range of configurations, as they may be more appropriate for other types devices. A variety of wire widths and periods were evaluated using Computer Simulation Technology Microwave Studio (CST MWS), and additional details are provided in the Supporting Information. The power transmitted at 1 THz through different configurations is provided in Figure 1A.[38] In general, THz transmission

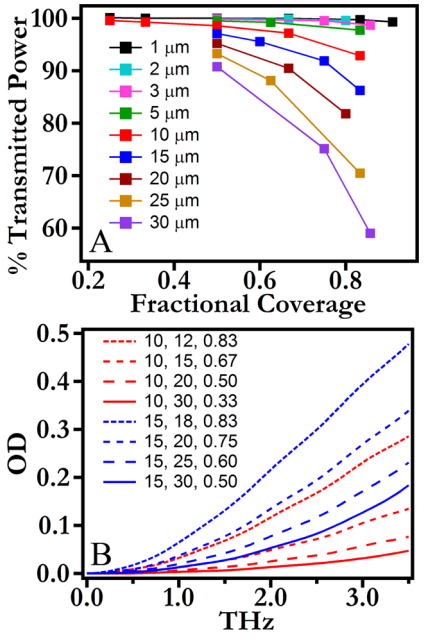

Figure 1. (A) Simulated power transmission at 1 THz through patterned FTO where the THz polarization is perpendicular to the direction of the wires. Transmission for various wire widths are shown as a function of fractional coverage (width/period). (B) Simulated optical density spectra for selected configurations with differing wire widths and periods in microns. The legend displays the width, period, and fractional coverage, respectively. A quartz substrate is used as a reference to take into account losses resulting from the substrate.

decreases as the wire width increases. For wire widths below 5 μm, increase in fractional coverage (defined as the width/period ratio) causes a negligible decrease in THz transmission. However, for larger widths, higher factional coverage has a much greater impact on the THz transmission. Similarly, THz attenuation with increasing frequency is also more severe for wider wires and higher factional coverage (Figure 1B). Choice of wire-grid configuration will depend on the transmission requirements as well as the type of device to be studied. In this report, the 15 μm:20 μm (width:period) configuration was chosen because the feature sizes are sufficiently large to enable etching of the FTO by either reactive ion etching or a solution-based method. This pattern was also selected for its large fractional coverage, which minimizes losses in electron collection efficiency at the FTO−metal oxide interface.

FTO/quartz substrates were patterned into a 15 μm:20 μm wire-grid configuration using standard lithography methods (Scheme 1). A thin layer of photoresist was applied to the FTO surface and exposed to UV light through a photomask. The UV-exposed portions of the photoresist were removed via immersion in a developer solution to reveal unprotected/

Scheme 1. Depiction of Photolithography Process Used to Make Patterned FTO (Green) on Fused Quartz (Grey) Substrates Using Photoresist (Red)[a]

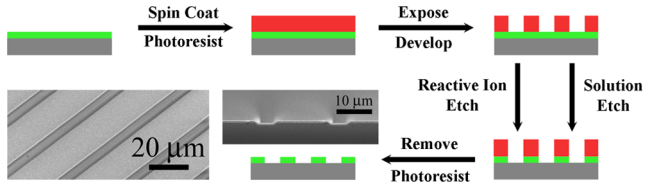

[a]SEM images demonstrate that the desired pattern was obtained.

exposed FTO. The unprotected FTO was then removed by two different etching methods to produce the desired wire-grid pattern. The first consisted of a reactive-ion etch treatment in the presence of an argon/chlorine plasma,[39] and the second consisted of a facile, solution based technique.[40] While both etching techniques successfully removed exposed FTO regions, the reactive-ion etching method was deemed superior, as it led to more homogeneous and reproducible results (c.f. Figure S2). The solution based technique is stated to be incompatible with features below 6 μm;[40] however, it worked well for FTO wires with a width of 15 μm spaced by 5 μm. SEM images of the patterned FTO/quartz substrates confirm that the desired wire width of 15 μm and wire period of 20 μm were obtained.

Figure 2 shows THz pulses propagated through a 1 mm thick fused quartz substrate as well as 15 μm:20 μm patterned and unpatterned (continuous) FTO layers on quartz. The THz transmission through the patterned substrate is highly dependent on the orientation of the FTO wires with respect to the

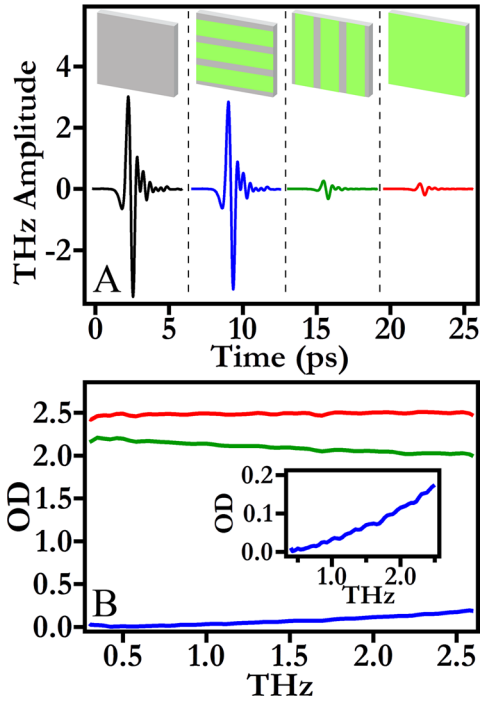

Figure 2. (A) THz pulses propagated though a blank quartz substrate (black), 15 μm:20 μm patterned FTO/quartz with wires oriented perpendicular (blue) and parallel (green) to THz polarization, and unpatterned FTO/quartz (red). Pulses are horizontally offset for clarity. (B) Optical density of patterned (perpendicular expanded in inset) and unpatterned FTO/quartz relative to a blank quartz substrate.

DOI: 10.1021/acs.jpclett.5b01473
J. Phys. Chem. Lett. 2015, 6, 3257−3262

polarization of the THz pulse. Just as with a wire-grid polarizer, transmission is high (~93% transmitted power at 1 THz) when the wires are perpendicular to the THz polarization, and low (0.3% transmitted power at 1 THz) when they are parallel. In the perpendicular orientation, the THz pulse propagated through FTO wires has ~15-fold greater amplitude and therefore much lower optical density compared with its unpatterned counterpart (Figure 2B).

Dye-sensitized solar cells (DSSCs) are produced by depositing a mesoporous dye-sensitized metal oxide film, such as TiO_2, onto a TCO electrode serving as photoanode, and using a platinized TCO electrode as cathode. A sandwich structure with an electrolyte solution containing a redox shuttle (in this case I^-/I_3^- dissolved in acetonitrile, along with other additives) filling the interior completes the electrical circuit. DSSCs were constructed using 15 μm:20 μm patterned FTO/quartz substrates as the TCO electrodes for both anode and cathode. Terahertz time domain measurements shown in Figure 3A confirm that the transmitted THz pulse amplitude through the complete DSSC constructed with patterned electrodes is over 150× that through a DSSC with continuous electrodes (which corresponds to a factor of over 25,000 higher power transmission at 1 THz). The optical density, shown in Figure 3B, increases with increasing frequency for both devices, and is due to absorption in the 1 mm thick fused quartz substrates as well as the electrolyte solution with a path length of 25 μm (c.f. Figure S5). While one may choose to use crystalline quartz as substrates to mitigate THz absorption at higher frequencies,[41] we find that the transmitted THz amplitude through full devices with patterned FTO on fused quartz substrates (~20% transmitted power at 1 THz) is sufficient to enable TRTS experiments with satisfactory signal-to-noise ratio. Figure 3A reveals that the DSSC device components (FTO wires, sensitized titanium dioxide film, and electrolyte) reduce the THz pulse amplitude by only ~40% relative to a THz pulse transmitted through a pair of quartz substrates alone.

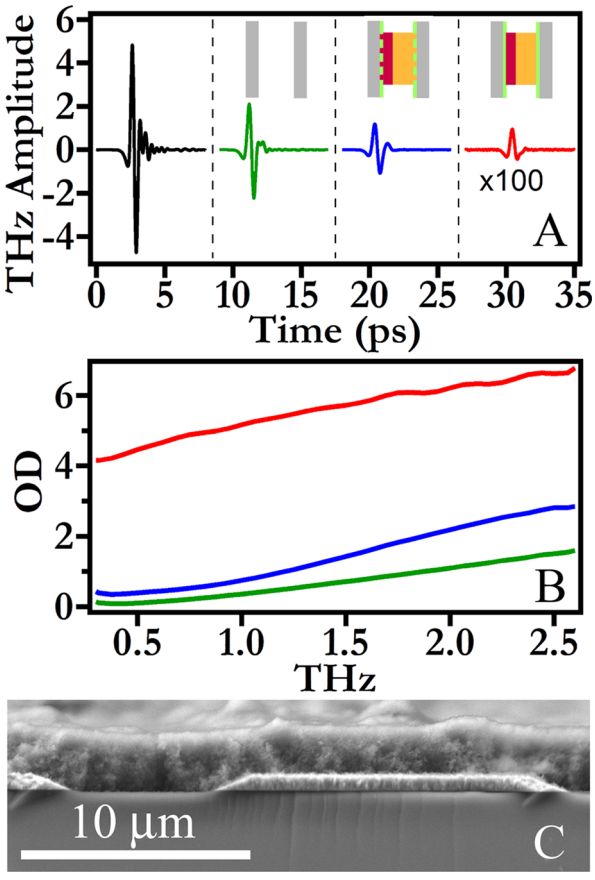

Figure 3. (A) Terahertz pulses propagated through DSSCs with 15 μm:20 μm patterned electrodes (blue) and with continuous FTO electrodes (red) as well as through air (black) and quartz substrates (green). (B) Optical density relative to the reference shown in black. (C) SEM image of the photoelectrochemical interface between a TiO_2 nanoparticulate film and the patterned electrode.

While THz-transparency of the full device is dramatically increased, device efficiency suffers to a small degree. Devices constructed with 15 μm:20 μm patterned electrodes had efficiencies averaging 2.6 ± 0.4% compared to 3.4 ± 0.4% for devices with continuous FTO electrodes. It must be noted that the purpose of the patterned electrodes is not to increase device efficiency, but rather to allow full devices to be probed with THz spectroscopy. Decreased short circuit current densities (8.1 ± 0.2 compared to 8.5 ± 0.5 mA/cm^2) are likely caused by losses in electron collection at the photoelectrochemcial interface shown in Figure 3C. While only the 15 μm:20 μm configuration electrodes were used to make devices, other configurations with decreased wire spacing may lead to higher efficiency while retaining THz-transparency. For instance, a 1 μm:2 or 3 μm:4 μm configuration is expected to minimize electron collection losses, and based on CST MWS simulations, will not affect the THz-transparency.

DSSCs constructed with 15 μm:20 μm patterned electrodes were probed via TRTS under an applied bias as well as continuous broadband illumination. Figure 4A shows TRTS traces for a device under four different biases along the photodiode region of the current−voltage curve: short circuit (0 V, SC), the maximum power point (−0.445 V, MPP), −0.6 V, and at open circuit (OC). There are clear differences in both electron injection efficiency, which is reflected in the magnitude of the maximum change in THz amplitude, as well as electron trapping dynamics, which result in the change in THz transmission returning to zero. Electron trapping dynamics are quantified by fitting eq 1 to the measured THz transient absorption.

$$\Delta\mathrm{THz} = -\left\{A \exp\left[\frac{-t}{\tau_{\mathrm{trap}}}\right] + y_0\right\} \quad (1)$$

The trapping time constant for electrons within the nanoparticulate TiO_2 film is denoted τ_{trap}, and t is the amount of time elapsed after the largest decrease in THz transmission has occurred. The offset term y_0 represents long-lived charge carriers with lifetimes on the nanoseconds−microseconds time scale that remain in the conduction band beyond the 600 ps window of the TRTS experiment. The overall electron injection efficiency into the conduction band (CB) is the sum of A and y_0. Figure 4B provides a graphical representation of the fitting parameters of eq 1 for TRTS measurements with and without continuous broadband illumination. The values are presented in Table 1.

The trends in trapping dynamics can be understood as a result of the modulation of the metal oxide Fermi level. Previous studies have shown that a negative applied bias shifts the Fermi level to more negative potentials (higher energies), and therefore midband trap states that lie below the metal oxide

DOI: 10.1021/acs.jpclett.5b01473
J. Phys. Chem. Lett. 2015, 6, 3257−3262

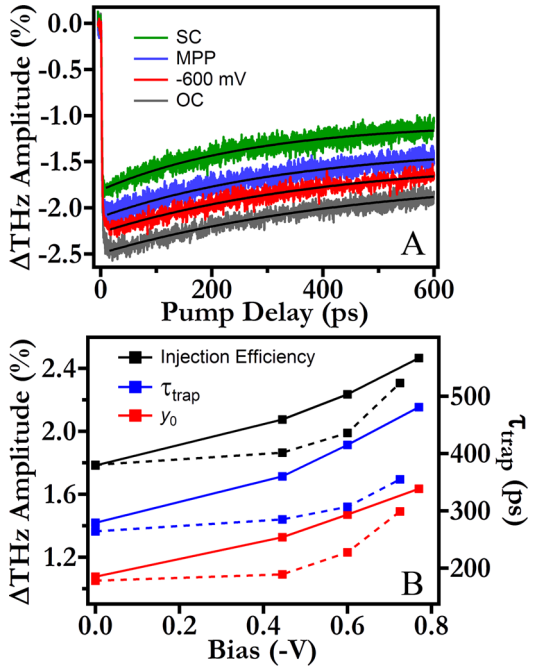

Figure 4. (A) TRTS measurements and fits showing the change in THz amplitude as a function of pump−probe delay for selected points along the current−voltage curve under continuous broadband illumination. Short circuit: green; maximum power point: blue; −600 mV: red; open circuit: dark gray. (B) Plot of parameters describing TRTS scans of a DSSC under an applied bias, with and without background illumination (solid lines and dashed lines, respectively). Injection efficiency and y_0 are in units of percent change in THz amplitude and values are given on the left axis. Trapping time constant τ_{trap} has units of picoseconds, and values are given on the right axis.

CB become occupied with electrons.[42] Similarly, illumination also shifts the Fermi level toward more negative potentials. We observe a decrease in electron trapping rate with increased negative bias and with illumination. These results suggest that the electron trapping rate depends on the occupation of trap states: a larger fraction of occupied trap states correlates to larger trapping time constants (meaning longer lifetimes of CB electrons). We must highlight that the electron trapping observed here is distinctly different than electron recombination studied by transient absorption spectroscopy.[36] Electron trapping is the relaxation of mobile CB electrons into midband nonmobile trap states, whereas recombination is the process of injected electrons returning to the oxidized dye.

We also find that electron injection into the CB is dependent on the metal oxide Fermi level in a similar manner: increased occupation of trap states leads to increased injection amplitude into the CB. This finding contrasts previous studies of injection efficiency where injection efficiency was found to be invariant over the bias potentials applied here.[35,42] Those studies, however, employed methods that cannot distinguish between metal oxide CB and trap states. Our observed changes in electron injection amplitude as a function of Fermi level are due to injection directly into trap states. Since electrons in these states are not mobile, they do not contribute to the TRTS signal. With increased occupancy of trap states under a larger negative bias, a larger portion of injected electrons are injected into the CB resulting in a larger change in transmitted THz amplitude.

Under short circuit conditions, there is very little change between TRTS traces with and without background illumination, as seen in Figure 4B. Previous findings reveal that the trap state distribution decreases exponentially with decreasing energy.[43] Thus, under short circuit conditions, the density of trap states is low, and it is expected that changes in bias voltage will result in negligible changes to the trapping dynamics since most of the trap states localized near the conduction band remain unoccupied. This is consistent with previous transient absorption studies, which have found that there is an onset potential, the more positive of which injection/recombination kinetics become bias independent.[37,42] Collectively, our results demonstrate that TRTS can be a powerful method to examine the photoexcited carrier dynamics in the conduction band of a metal oxide, and provides new insights into the illumination and bias dependence of electron injection and trapping in a functioning device.

We have demonstrated that devices utilizing transparent conductive oxides as electrodes can be probed with THz spectroscopy by modifying them to mimic wire-grid polarizers. We have manufactured 15 μm:20 μm FTO electrodes using standard photolithography and two different etching methods. These patterned electrodes were employed in dye-sensitized solar cells, which were probed with TRTS to reveal changes in electron injection efficiency and trapping resulting from the application of an applied voltage and broadband illumination. While the method utilizing THz-transparent electrodes to study devices may apply to many types of devices, our future work will primarily focus on photoelectrochemical and photocatalytic cells. Specifically, we intend to elucidate in detail how changes in the electronic structure of the metal oxide affects electron injection efficiency/dynamics as well as electron trapping dynamics.

Table 1. Fitting Parameters for Trapping Dynamics Measured under Various Applied Biases with and without Continuous (CW) Broadband Illumination

	injection amplitude[a]		y_0[a]		τ_{trap} (ps)	
applied bias	with CW illumination	without CW illumination	with CW illumination	without CW illumination	with CW illumination	without CW illumination
0 mV	1.78	1.79	1.08	1.05	279	264
445 mV	2.08	1.87	1.33	1.09	360	285
600 mV	2.24	1.99	1.47	1.23	415	307
OC[b]	2.47	2.31	1.64	1.49	481	355

[a]Injection amplitude is taken to be the sum of y_0 and A in eq 1 (all in units of percent change in THz amplitude). [b]Open circuit condition was obtained by setting the device current to 0 A.

DOI: 10.1021/acs.jpclett.5b01473
J. Phys. Chem. Lett. 2015, 6, 3257−3262

EXPERIMENTAL METHODS

The THz spectrometer and data acquisition methods are described in the Supporting Information, and additional details are found in ref 2. Similarly, the details for lithographically patterning FTO electrodes and DSSC fabrication are found in the Supporting Information.

ASSOCIATED CONTENT

Supporting Information

Additional details of CST simulations, FTO etching methods, DSSC fabrication, and time-resolved THz spectroscopy setup. THz optical density of DSSC components and representative current−voltage curves of a DSSC with patterned electrodes, as well as solar cell parameters for devices with and without patterned electrodes. The Supporting Information is available free of charge on the ACS Publications website at DOI: 10.1021/acs.jpclett.5b01473.

(PDF)

AUTHOR INFORMATION

Corresponding Author

*E-mail: charles.schmuttenmaer@yale.edu.

Notes

The authors declare no competing financial interest.

ACKNOWLEDGMENTS

This work was funded by the U.S. Department of Energy Office of Science, Office of Basic Energy Sciences, under award no. DE-FG02-07ER15909 and by a generous donation from the TomKat Charitable Trust. We also acknowledge Stafford W. Sheehan for assistance with scanning electron microscopy and helpful discussions, as well as Michael Power for advice and assistance on photolithography techniques.

REFERENCES

(1) Beard, M. C.; Turner, G. M.; Schmuttenmaer, C. A. Terahertz Spectroscopy. *J. Phys. Chem. B* **2002**, *106*, 7146−7159.
(2) Beard, M. C.; Turner, G. M.; Schmuttenmaer, C. A. Transient Photoconductivity in GaAs as Measured by Time-Resolved Terahertz Spectroscopy. *Phys. Rev. B: Condens. Matter Mater. Phys.* **2000**, *62*, 15764−15777.
(3) Huber, R.; Tauser, F.; Brodschelm, A.; Bichler, M.; Abstreiter, G.; Leitenstorfer, A. How Many-Particle Interactions Develop After Ultrafast Excitation of an Electron-Hole Plasma. *Nature* **2001**, *414*, 286−289.
(4) Knoesel, E.; Bonn, M.; Shan, J.; Heinz, T. F. Charge Transport and Carrier Dynamics in Liquids Probed by THz Time-Domain Spectroscopy. *Phys. Rev. Lett.* **2001**, *86*, 340−343.
(5) Shan, J.; Wang, F.; Knoesel, E.; Bonn, M.; Heinz, T. F. Measurement of the Frequency-Dependent Conductivity in Sapphire. *Phys. Rev. Lett.* **2003**, *90*, 247401.
(6) Kaindl, R. A.; Carnahan, M. A.; Hägele, D.; Lövenich, R.; Chemla, D. S. Ultrafast Terahertz Probes of Transient Conducting and Insulating Phases in an Electron-Hole Gas. *Nature* **2003**, *423*, 734−738.
(7) Hendry, E.; Wang, F.; Shan, J.; Heinz, T. F.; Bonn, M. Electron Transport in TiO_2 Probed by THz Time-Domain Spectroscopy. *Phys. Rev. B: Condens. Matter Mater. Phys.* **2004**, *69*, 081101.
(8) Hendry, E.; Koeberg, M.; Schins, J. M.; Nienhuys, H. K.; Sundström, V.; Siebbeles, L. D. A.; Bonn, M. Interchain Effects in the Ultrafast Photophysics of a Semiconducting Polymer: THz Time-Domain Spectroscopy of Thin Films and Isolated Chains in Solution. *Phys. Rev. B: Condens. Matter Mater. Phys.* **2005**, *71*, 125201.
(9) Baxter, J. B.; Schmuttenmaer, C. A. Conductivity of ZnO Nanowires, Nanoparticles, and Thin Films Using Time-Resolved Terahertz Spectroscopy. *J. Phys. Chem. B* **2006**, *110*, 25229−25239.
(10) Němec, H.; Kužel, P.; Sundström, V. Charge Transport in Nanostructured Materials for Solar Energy Conversion Studied by Time-Resolved Terahertz Spectroscopy. *J. Photochem. Photobiol., A* **2010**, *215*, 123−139.
(11) Ulbricht, R.; Hendry, E.; Shan, J.; Heinz, T. F.; Bonn, M. Carrier Dynamics in Semiconductors Studied with Time-Resolved Terahertz Spectroscopy. *Rev. Mod. Phys.* **2011**, *83*, 543−586.
(12) Milot, R. L.; Moore, G. F.; Crabtree, R. H.; Brudvig, G. W.; Schmuttenmaer, C. A. Electron Injection Dynamics from Photoexcited Porphyrin Dyes into SnO_2 and TiO_2 Nanoparticles. *J. Phys. Chem. C* **2013**, *117*, 21662−21670.
(13) Ai, X.; Beard, M. C.; Knutsen, K. P.; Shaheen, S. E.; Rumbles, G.; Ellingson, R. J. Photoinduced Charge Carrier Generation in a Poly(3-Hexylthiophene) and Methanofullerene Bulk Heterojunction Investigated by Time-Resolved Terahertz Spectroscopy. *J. Phys. Chem. B* **2006**, *110*, 25462−25471.
(14) Cunningham, P. D.; Hayden, L. M. Carrier Dynamics Resulting from Above and Below Gap Excitation of P3HT and P3HT/PCBM Investigated by Optical-Pump Terahertz-Probe Spectroscopy. *J. Phys. Chem. C* **2008**, *112*, 7928−7935.
(15) Esenturk, O.; Melinger, J. S.; Heilweil, E. J. Terahertz Mobility Measurements on Poly-3-Hexylthiophene Films: Device Comparison, Molecular Weight, and Film Processing Effects. *J. Appl. Phys.* **2008**, *103*, 023102.
(16) Němec, H.; Nienhuys, H. K.; Zhang, F.; Inganas, O.; Yartsev, A.; Sundström, V. Charge Carrier Dynamics in Alternating Polyfluorene Copolymer: Fullerene Blends Probed by Terahertz Spectroscopy. *J. Phys. Chem. C* **2008**, *112*, 6558−6563.
(17) Ponseca, C. S.; Yartsev, A.; Wang, E.; Andersson, M. R.; Vithanage, D.; Sundström, V. Ultrafast Terahertz Photoconductivity of Bulk Heterojunction Materials Reveals High Carrier Mobility up to Nanosecond Time Scale. *J. Am. Chem. Soc.* **2012**, *134*, 11836−11839.
(18) Brauer, J. C.; Thorsmølle, V. K.; Moser, J.-E. Terahertz Time-Domain Spectroscopy Study of the Conductivity of Hole-Transporting Materials. *Chimia* **2009**, *63*, 189−192.
(19) Poddutoori, P. K.; Thomsen, J. M.; Milot, R. L.; Sheehan, S. W.; Negre, C. F. A.; Garapati, V. K. R.; Schmuttenmaer, C. A.; Batista, V. S.; Brudvig, G. W.; van der Est, A. Interfacial Electron Transfer in Photoanodes Based on Phosphorus(V) Porphyrin Sensitizers Co-Deposited on SnO_2 with the Ir(III)Cp* Water Oxidation Precatalyst. *J. Mater. Chem. A* **2015**, *3*, 3868−3879.
(20) Martini, L. A.; Moore, G. F.; Milot, R. L.; Cai, L. Z.; Sheehan, S. W.; Schmuttenmaer, C. A.; Brudvig, G. W.; Crabtree, R. H. Modular Assembly of High-Potential Zinc Porphyrin Photosensitizers Attached to TiO_2 with a Series of Anchoring Groups. *J. Phys. Chem. C* **2013**, *117*, 14526−14533.
(21) McNamara, W. R.; Snoeberger, R. C., III; Li, G.; Richter, C.; Allen, L. J.; Milot, R. L.; Schmuttenmaer, C. A.; Crabtree, R. H.; Brudvig, G. W.; Batista, V. S. Hydroxamate Anchors for Water-Stable Attachment to TiO_2 Nanoparticles. *Energy Environ. Sci.* **2009**, *2*, 1173−1175.
(22) Negre, C. F. A.; Milot, R. L.; Martini, L. A.; Ding, W.; Crabtree, R. H.; Schmuttenmaer, C. A.; Batista, V. S. Efficiency of Interfacial Electron Transfer from Zn-Porphyrin Dyes into TiO_2 Correlated to the Linker Single Molecule Conductance. *J. Phys. Chem. C* **2013**, *117*, 24462−24470.
(23) Turner, G. M.; Beard, M. C.; Schmuttenmaer, C. A. Carrier Localization and Cooling in Dye-Sensitized Nanocrystalline Titanium Dioxide. *J. Phys. Chem. B* **2002**, *106*, 11716−11719.
(24) Moore, G. F.; Konezny, S. J.; Song, H.-e.; Milot, R. L.; Blakemore, J. D.; Lee, M. L.; Batista, V. S.; Schmuttenmaer, C. A.; Crabtree, R. H.; Brudvig, G. W. Bioinspired High-Potential Porphyrin Photoanodes. *J. Phys. Chem. C* **2012**, *116*, 4892−4902.
(25) Pijpers, J. J. H.; Ulbricht, R.; Derossi, S.; Reek, J. N. H.; Bonn, M. Picosecond Electron Injection Dynamics in Dye-Sensitized Oxides in the Presence of Electrolyte. *J. Phys. Chem. C* **2011**, *115*, 2578−2584.

DOI: 10.1021/acs.jpclett.5b01473
J. Phys. Chem. Lett. 2015, 6, 3257−3262

(26) Němec, H.; Kužel, P.; Kadlec, F.; Fattakhova-Rohlfing, D.; Szeifert, J.; Bein, T.; Kalousek, V.; Rathouský, J. Ultrafast Terahertz Photoconductivity in Nanocrystalline Mesoporous TiO_2 films. *Appl. Phys. Lett.* **2010**, *96*, 062103.
(27) Tiwana, P.; Docampo, P.; Johnston, M. B.; Herz, L. M.; Snaith, H. J. The Origin of an Efficiency Improving "Light Soaking" Effect in SnO_2 Based Solid-State Dye-Sensitized Solar Cells. *Energy Environ. Sci.* **2012**, *5*, 9566−9573.
(28) Němec, H.; Rochford, J.; Taratula, O.; Galoppini, E.; Kužel, P.; Polívka, T.; Yartsev, A.; Sundström, V. Influence of the Electron-Cation Interaction on Electron Mobility in Dye-Sensitized ZnO and TiO_2 Nanocrystals: A Study Using Ultrafast Terahertz Spectroscopy. *Phys. Rev. Lett.* **2010**, *104*, 197401.
(29) Wehrenfennig, C.; Liu, M.; Snaith, H. J.; Johnston, M. B.; Herz, L. M. Charge-Carrier Dynamics in Vapour-Deposited Films of the Organolead Halide Perovskite $CH_3NH_3PbI_{3-x}Cl_x$. *Energy Environ. Sci.* **2014**, *7*, 2269−2275.
(30) Wehrenfennig, C.; Eperon, G. E.; Johnston, M. B.; Snaith, H. J.; Herz, L. M. High Charge Carrier Mobilities and Lifetimes in Organolead Trihalide Perovskites. *Adv. Mater.* **2014**, *26*, 1584−1589.
(31) Marchioro, A.; Brauer, J. C.; Teuscher, J.; Grätzel, M.; Moser, J. E. Photoinduced Processes in Lead Iodide Perovskite Solid-State Solar Cells. *Physical Chemistry of Interfaces and Nanomaterials XII* **2013**, *8811*, 881108.
(32) Bauer, T.; Kolb, J. S.; Löffler, T.; Mohler, E.; Roskos, H. G.; Pernisz, U. C. Indium-Tin-Oxide-Coated Glass as Dichroic Mirror for Far-Infrared Electromagnetic Radiation. *J. Appl. Phys.* **2002**, *92*, 2210−2212.
(33) Li, C. H.; Koenigsmann, C.; Ding, W. D.; Rudshteyn, B.; Yang, K. R.; Regan, K. P.; Konezny, S. J.; Batista, V. S.; Brudvig, G. W.; Schmuttenmaer, C. A.; Kim, J. H. Facet-Dependent Photoelectrochemical Performance of TiO_2 Nanostructures: An Experimental and Computational Study. *J. Am. Chem. Soc.* **2015**, *137*, 1520−1529.
(34) Abrusci, A.; Santosh Kumar, R. S.; Al-Hashimi, M.; Heeney, M.; Petrozza, A.; Snaith, H. J. Influence of Ion Induced Local Coulomb Field and Polarity on Charge Generation and Efficiency in Poly(3-Hexylthiophene)-Based Solid-State Dye-Sensitized Solar Cells. *Adv. Funct. Mater.* **2011**, *21*, 2571−2579.
(35) Koops, S. E.; O'Regan, B. C.; Barnes, P. R. F.; Durrant, J. R. Parameters Influencing the Efficiency of Electron Injection in Dye-Sensitized Solar Cells. *J. Am. Chem. Soc.* **2009**, *131*, 4808−4818.
(36) Haque, S. A.; Tachibana, Y.; Klug, D. R.; Durrant, J. R. Charge Recombination Kinetics in Dye-Sensitized Nanocrystalline Titanium Dioxide Flms Under Externally Applied Bias. *J. Phys. Chem. B* **1998**, *102*, 1745−1749.
(37) Haque, S. A.; Tachibana, Y.; Willis, R. L.; Moser, J. E.; Grätzel, M.; Klug, D. R.; Durrant, J. R. Parameters Influencing Charge Recombination Kinetics in Dye-Sensitized Nanocrystalline Titanium Dioxide Films. *J. Phys. Chem. B* **2000**, *104*, 538−547.
(38) It is worth reminding the reader that we measure the amplitude of the oscillating electromagnetic THz field. Sometimes it makes more sense to describe a property at the amplitude, or field level, and other times at the intensity level. In the latter case, we Fourier transform the time-domain THz waveform and analyze the effects on the power spectrum. We have made it clear throughout this Letter when we are referring to amplitude, and when we are referring to power.
(39) Kong, S. M.; Xiao, Y.; Kim, K. H.; Lee, W. I.; Chung, C. W. Performance Improvement of Dye-Sensitized Solar Cells by Surface Patterning of Fluorine-Doped Tin Oxide Transparent Electrodes. *Thin Solid Films* **2011**, *519*, 3173−3176.
(40) McLean, D.; Feldman, B. Method for Etching. United States Patent 5,976,396, 1999.
(41) Grischkowsky, D.; Keiding, S.; van Exter, M.; Fattinger, C. Far-Infrared Time-Domain Spectroscopy with Terahertz Beams of Dielectrics and Semiconductors. *J. Opt. Soc. Am. B* **1990**, *7*, 2006−2015.
(42) Tachibana, Y.; Haque, S. A.; Mercer, I. P.; Moser, J. E.; Klug, D. R.; Durrant, J. R. Modulation of the Rate of Electron Injection in Dye-Sensitized Nanocrystalline TiO_2 Films by Externally Applied Bias. *J. Phys. Chem. B* **2001**, *105*, 7424−7431.
(43) Frank, A. J.; Kopidakis, N.; van de Lagemaat, J. Electrons in Nanostructured TiO_2 Solar Cells: Transport, Recombination and Photovoltaic Properties. *Coord. Chem. Rev.* **2004**, *248*, 1165−1179.

DOI: 10.1021/acs.jpclett.5b01473
J. Phys. Chem. Lett. 2015, 6, 3257−3262